

**BIO-INSPIRED SYNTHESIS OF MIXED-PHASE Fe_2O_3
MAGNETIC NANORODS AS A NOVEL RECOVERABLE
HETEROGENEOUS CATALYST FOR
BIGINELLI SYNTHESIS**

**THE PROJECT SUBMITTED TO
SAVITRIBAI PHULE PUNE UNIVERSITY, PUNE (M.S)
FOR THE AWARD OF M.Sc. ORGANIC CHEMISTRY IN THE
FACULTY OF SCIENCE & TECHNOLOGY**

**SUBMITTED BY
MR. ROHIT ASHOK SHINDE**

**UNDER THE GUIDANCE OF
MR. DNYANESHWAR SANAP**

**ASSISTANTS PROFESSOR , DEPARTMENT OF CHEMISTRY
G.M.D. ARTS, B.W. COMMERCE AND SCIENCE
COLLEGE, SINNAR, TAL-SINNAR, DIST-NASHIK - 422103**

**WORK PLACE
POST GRADUATE DEPARTMENT OF CHEMISTRY
AND RESEARCH CENTER,
G.M.D. ARTS, B.W. COMMERCE AND SCIENCE
COLLEGE, SINNAR, TAL-SINNAR, DIST-NASHIK - 422103**

APRIL -MAY 2023



MARATHA VIDYA PRASARAK SAMAJ, NASHIK

**G.M.D. ARTS, B.W. COMMERCE AND SCIENCE
COLLEGE, SINNAR, TAL-SINNAR, DIST-NASHIK - 422103**

CERTIFICATE

DEPARTMENT OF CHEMISTRY

This is to certify that the work incorporated in the project entitled

Bio-inspired synthesis of mixed-phase Fe_2O_3 magnetic nanorods as a novel recoverable heterogeneous catalyst for Biginelli Synthesis

Was satisfactorily carried out by **Mr. Rohit Ashok Shinde** of **M.Sc. Organic Chemistry**. He has completed this project under my supervision and guidance during **Academic Year 2022-2023**. This project work submitted by his original and the scientific information obtain from other sources have been duly acknowledged.

Mr. Dnyaneshwar Sanap
(Project Guide)



Maratha Vidya Prasarak Samaj's
G.M.D. ARTS, COMMERCE AND SCIENCE COLLEGE,
SINNAR DIST. NASHIK
DEPARTMENT OF CHEMISTRY (PG)

CERTIFICATE

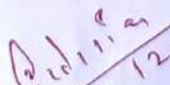
This is to certify that **Mr. Shinde Rohit Ashok** of M.Sc. II (Organic Chemistry) has satisfactorily completed the project work in **Organic Chemistry** during the semester IV of academic year 2022-2023.


Date : 12-05-2023


Place : Sinnar




Project Incharge


12.05.2023
Examiner


HoD Chemistry
HEAD


Principal

DEPARTMENT OF CHEMISTRY
G.M.D. Arts, B.W. Commerce and Science college, Sinnar
PRINCIPAL
G.M.D. Arts, B.W. Commerce and Science College, Sinnar, Dist. Nashik

ACKNOWLEDGEMENT

- I would like to thank M.V.P. Samaj's G.M.D. Arts B.W. Commerce and Science College Sinnar, for providing me with the necessary resources, infrastructural, and facilities to carry out this project.
- I would like to thank our College Principle **Dr. P. V. Rasal** for constant support and providing infrastuctural facility for this project work.
- I would like to thank, HoD Prof. M.R. Gaware for his constructive help during project.
- I would like to thank, **Mr. Dnyaneshwar Sanap** (Project Guide), for their constant encouragement, insightful feedback, and expert guidance that helped me to navigate through the various challenges of this project.
- I would like to thank all the faculty members of the Department of Chemistry, for imparting me with the theoretical and practical knowledge necessary to complete this project.
- I would like to thank my classmates and colleagues, for their feedback, suggestions, and stimulating discussions that enriched my understanding of the subject matter.

Shinde

Shinde Rohit Ashok.

Table of Content

➤ Abstract	1
1. Introduction	1
2. Experimental	2
2.1 Chemical/materials	2
2.2 Preparation of leaves extracts	3
2.3 Synthesis of Fe ₂ O ₃ Magnetic NRs	3
2.4 General procedure for ethyl 1,2,3,4-tetrahydro-6-methyl-2-oxo-4-arylpyrimidine-5- carboxylate synthesis	3
2.5 Fe ₂ O ₃ MNRs characterization technique	4
3. Result and discussion	4
3.1 Physical, chemical, and structural characterization of the catalyst	4
3.2 Synthesis of ethyl 1,2,3,4-tetrahydro-6-methyl-2-oxo-4-arylpyrimidine-5-carboxylate derivative	11
3.3 Probable mechanistic pathway of the reaction	17
4. Conclusion	18
➤ References	18

Bio-inspired synthesis of mixed-phase Fe₂O₃ magnetic nanorods as a novel recoverable heterogeneous catalyst for Biginelli synthesis

Abstract

For the first time, mixed-phase (Hematite and Maghemite) magnetic Fe₂O₃ nanorods were successfully biosynthesized by sol-gel auto-combustion method using the 1:1 mixture of *Eucalyptus citriodora* and *Murraya koenigii* leaf extract as a capping agent, and its catalytic effect on synthesis of ethyl 1,2,3,4-tetrahydro-6-methyl-2-oxo-4-arylpyrimidine-5-carboxylate (THPMs) derivatives were investigated. Further, the phase formation, surface topography, and crystallinity of biosynthesized Fe₂O₃ nanorods (NRs) were explored using powder XRD (X-Ray Diffraction), UVDRS (UV-Visible Reflectance Spectroscopy), FTIR (Fourier Transform Infrared Spectroscopy), FESEM (Field Emission Scanning Electron Microscopy), EDX (Energy Dispersive X-Ray), and VSM (Vibrating Sample Magnetometry). Furthermore, the catalytic activity of biosynthesized Fe₂O₃ NRs was examined for one-pot synthesis of ethyl 1,2,3,4-tetrahydro-6-methyl-2-oxo-4-arylpyrimidine-5-carboxylate *via* Biginelli reaction. To achieve high yields (93-99 %) of ethyl 1,2,3,4-tetrahydro-6-methyl-2-oxo-4-arylpyrimidine-5-carboxylate derivatives, this heterogeneous catalytic method is used with a wide range of aromatic aldehydes within a minimum reaction time, simple reaction work-up, and easily recoverable catalyst by an external magnet. The recovered catalyst is then employed for five successive cycles without non-noticeable loss of catalytic activity. We believe that this protocol presents a broad scope for Biginelli reaction through greenily produced and magnetically separable heterogeneous catalysts.

Keywords: Green synthesis; Biginelli reaction; Fe₂O₃ NRs; Heterogeneous catalysis

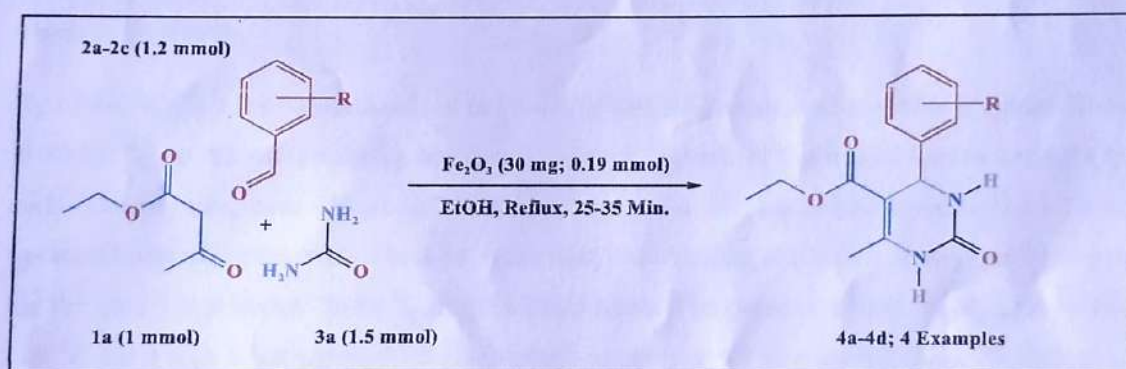
1. Introduction

The 2-oxo-1,2,3,4-tetrahydropyrimidines-THPMs (The former name is 3,4-dihydropyrimidin-2(1H)-ones-DHPMs) Safford's are an important class of heterocyclic compounds known for a wide range of biological activities including anti-HIV [1], antibacterial, antifungal, anti-tubercular, antioxidant, anti-inflammatory [2], and anticancer [3] as well as potential agents in the treatment of many diseases including diabetes, Alzheimer's disease [4, 5], and other neuros diseases [3].

THPMs are a unique scaffold for constructing and creating biologically important medicines and agents for anti-tumour [3], and Alzheimer's disease [4, 5] by changing the substituent on its C6 position.

Conventionally, the THPMs Safford's were synthesized by the well-known Biginelli reaction by three components reaction between aldehyde, ethyl acetoacetate, and urea assisted by hydrochloric acid as a homogeneous catalyst [6] with the yield of 72-92 %.

However, there are five major challenges embedded in the synthesis of THPMs Safford's: 1) use of hazardous solvents; 2) use of hazardous reagents; 3) low to moderate yield; 4) long reaction time; 5) recovery of homogenous catalyst. Herein, we report the successful synthesis strategy for the THPMs Safford's synthesis, using heterogeneous - magnetically separable biosynthesized Fe_2O_3 catalyst, with the yield in the range of 93-99 % (Scheme 1). The structure of the synthesized products was confirmed by ^1H NMR and ^{13}C NMR.



Scheme 1: Strategies for the construction of ethyl 1,2,3,4-tetrahydro-6-methyl-2-oxo-4-arylpyrimidine-5-carboxylate

2. Experimental

2.1 Chemical/materials

Eucalyptus citriodora (Nilgiri Plant Leaf), *Murraya koenigii* leaf (Curry Leaf), Ferric nitrate nonahydrate ($\text{Fe}(\text{NO}_3)_3 \cdot 9\text{H}_2\text{O}$), substituted aldehydes, ethyl alcohol, ethyl acetate, and n-hexane were purchased from S.D. Fine Chemical Limited. Before being used in this investigation, all the solvents were distilled off.

2.2 Preparation of leaves extracts

The fresh leaves of *Eucalyptus citriodora* and *Murraya koenigii* were collected from the campus of G.M.D. Arts B.W. Commerce and Science College Sinnar, Nashik (Maharashtra), were washed thoroughly with distilled water to remove mud, dirt, impurities, and surface contamination. The wash leaves were weighed accurately at 8 gm each, cut into small pieces and pulverized using the mixer in 10 mL distilled water separately. Transfer the pest to a 100 mL RB flask and add 30 mL of distilled water to each pest mixture, then gently heat at about 80-90 °C for 1 h, then cool it, and filter it with Whatman filter paper (No. 41). The obtained filtrates use for the synthesis of Fe₂O₃ NRs after mixing.

2.3 Synthesis of Fe₂O₃ Magnetic NRs

Fe₂O₃ Magnetic NRs were successfully fabricated by a simple sol-gel auto-combustion technique using the Fe(NO₃)₃·9H₂O, *Eucalyptus citriodora*, and *Murraya koenigii* leaves extract precursors.

5 g of Fe(NO₃)₃·9H₂O was dissolved in 15 mL of distilled water, and stir it for the next 30 min at 70-80 °C, to the same homogeneous salt solution, 50 mL of the mixed leaves extract (1:1) added drop by drop over 40 min at 70-80 °C, stirring of mixture was continued for next 30 min upon addition of leaves extract is over. After that, the resulting solution was kept on a hot plate for the next 3 h at about 70-80 °C to get a thick paste. The paste obtained was heated to 100-120 °C for 5 h in a hot air oven for auto-combustion to get a dried thick mass. Further dried mass, grind in mortar-pestle for 30 min to get dry powder. The obtained dried Fe₂O₃ powder was calcinated at 400 °C for 3 h. Finally, the dark reddish Brown Fe₂O₃ powder obtained. The obtained nanocrystalline Fe₂O₃ screen for the synthesis of ethyl 1,2,3,4-tetrahydro-6-methyl-2-oxo-4-arylpyrimidine-5-carboxylate-THPMs derivatives.

2.4 General procedure for ethyl 1,2,3,4-tetrahydro-6-methyl-2-oxo-4-arylpyrimidine-5-carboxylate synthesis

A mixture of freshly distilled Ethyl acetoacetate (1 mmol), aromatic carbaldehyde (1.2 mmol), Urea (1.5 mmol), and biosynthesized Fe₂O₃ NRs (0.19 mmol) in ethyl alcohol (3 mL) was well refluxed in a 25 mL RB flask under dark condition (Table No. 3, Entry 1 to 4). TLC was used to track the development of the reaction (using n-Hexane and Ethyl acetate in 1:1 proportion). Upon the completion of the reaction, the reaction mixture is kept near an external magnet for

5 to 7 min to separate the Fe_2O_3 catalyst, and then the ethanolic layer of the reaction mixture is separated by decanting into a beaker through Whatman filter paper. In the end, the catalyst in Et_2O was washed using 1 mL ethanol every time inrice, dried, activated, and used for a sequential cycle. After column chromatography, the pure product was obtained using n-hexane and ethyl acetate (85:15 to 40:60) solvent as a mobile phase. By using ^1H NMR, and ^{13}C NMR techniques, all the organic products were confirmed.

2.5 Fe_2O_3 NRs characterization technique

Model V-770 - Jasco Spectrophotometer was used to get a UV-DRS of Fe_2O_3 NRs. The UV-DRS absorption spectra were measured from 200 to 800 nm. A JASCO-4600, Type-A model spectrophotometer was used to acquire FT-IR spectra of NRs in the 400 to 4000 cm^{-1} range. Bruker D8 diffractometer having Cu-K α radiation (having $\lambda = 1.54060 \text{ \AA}$) with an angle between 20° to 80° , with a minimum step size of 2θ is 0.020° were carried out for crystal structure analysis of biosynthesized NRs. 10 kV accelerating voltage FEI Nova Nano SEM 450 instrument was used to examine cross-section morphology or surface structure and element mapping of NRs. Quanta-Chrome NOVA 1000e model instrument was used to acquire the data of N_2 adsorption-desorption, pore-sized distribution, and pore diameter at 77 K. The magnetic behavior of biosynthesized NRs was investigated using Vibrating Sample Magnetometry. Thiele's tube assembly measured the melting points of the synthesized ethyl 1,2,3,4-tetrahydro-6-methyl-2-oxo-4-arylpyrimidine-5-carboxylate scaffold. Finally, the Bruker Advance NEO 500 MHz Spectrometer was used to confirm the molecular structure of synthesized ethyl 1,2,3,4-tetrahydro-6-methyl-2-oxo-4-arylpyrimidine-5-carboxylate scaffold with the instrument strength of 500 MHz and 126 MHz for ^1H and ^{13}C nuclei, respectively.

3. Result and discussion

3.1 Physical, chemical, and structural characterization of the catalyst

The powder X-Ray Diffraction pattern of biosynthesized Fe_2O_3 demonstrates that the sample contains Hematite and Maghemite mixed phase, with rhombohedral and cubic crystal systems [8]. **Figure 1** revealed characteristic X-Ray Diffraction peaks at 2θ : 24.18 (110), 33.20 (211), 35.68 (101), 40.92 (210), 49.53 (202), 54.15 (312), 64.10 (211), 72.01 (433), and 26.18 (211), 30.23 (202), 35.72 (311), 43.42 (400), 46.20 (411), 57.44 (511), 63.01 (404), 74.66 (533) for Hematite and Maghemite phase respectively. This result of the mixed phase is in good agreement with previous studies for Hematite [9, 10] and Maghemite [11], respectively. The

average crystalline size of mixed-phase biosynthesized NRs was calculated using Scherrer's equation by Full Width at Half Maximum (FWHM) for prominent peaks, which were found to be 18.36 nm (Table 1).

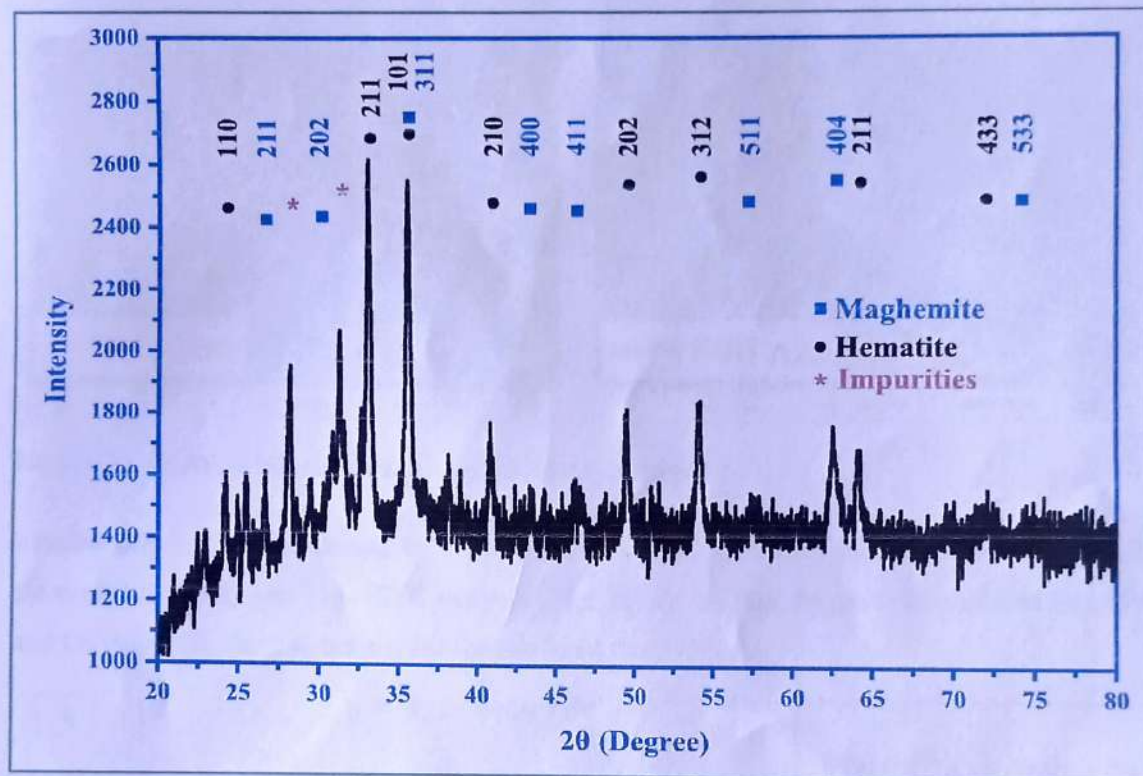


Figure 1: XRD patterns of biosynthesized Fe_2O_3 NRs

2θ (Degree)	FWHM	Crystalline Size D (nm)	Average D (nm)
24.20	4.5012	1.74	18.36
33.20	0.3323	24.12	
35.70	0.3734	21.61	
40.91	0.3421	23.96	
49.53	0.3521	24.02	
54.12	0.4462	19.33	
62.97	0.7046	12.76	
64.10	0.4688	19.33	

Table 1: Calculation of average crystal size of biosynthesized Fe_2O_3 NRs by Scherer equation using FWHM for listed prominent peaks

Further morphological characteristics, sizes, and element mapping of fabricated Fe_2O_3 NRs were studied by FESEM analysis, as shown in **Figure 2**. According to FESEM images, the rod-shaped morphology and uniform distribution were obtained Fig. 2(a-b) as-prepared NRs.

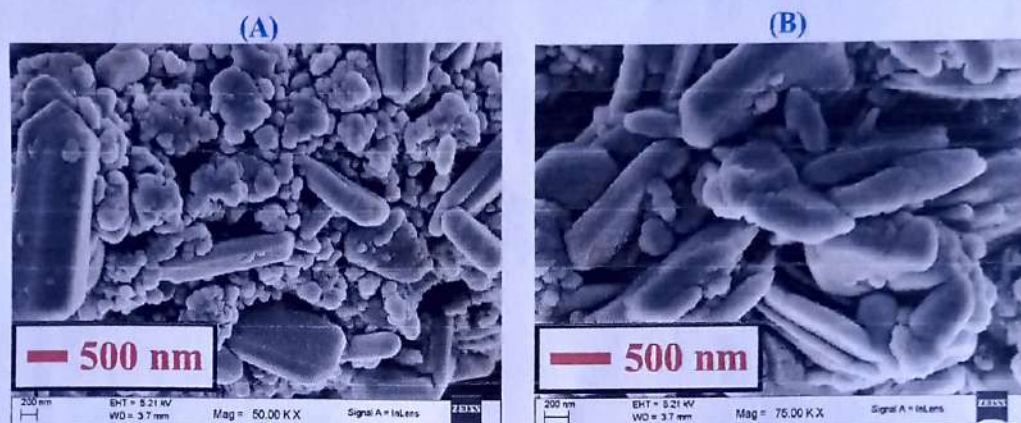


Figure 2: FE-SEM images of as-prepared Fe_2O_3 NRs (a-b).

Additionally, as demonstrated in **Figure 3a**, the EDX spectrum indicated the Fe_2O_3 NRs elemental composition. This EDX analysis (**Fig. 3b**) shows that the material contains Iron (Fe) and Oxygen (O), demonstrating the formation of Fe_2O_3 NRs.

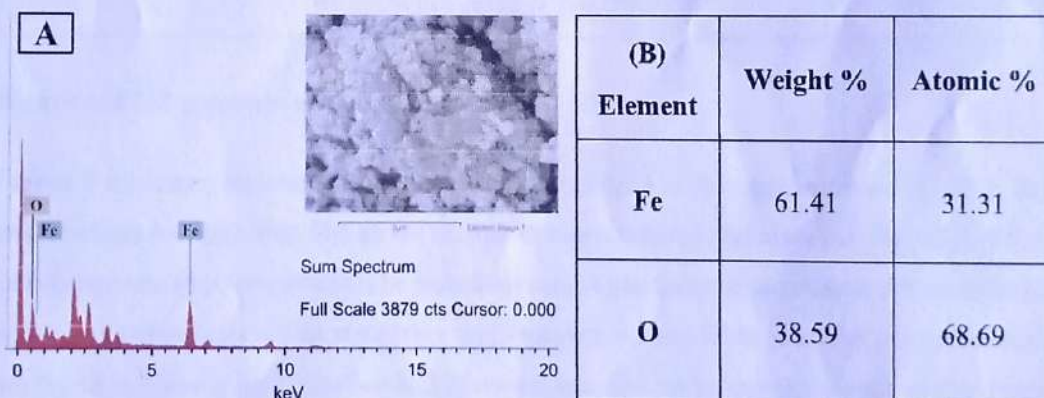


Figure 3: EDX spectrum of synthesized Fe_2O_3 NRs (a); Percent element composition of Fe_2O_3 NRs (b).

The FTIR spectrum was used to investigate the nature of chemical bonding in the molecule. **Figure 4**, FTIR spectrum of biosynthesized Fe_2O_3 NRs, shows intense absorption peaks at 1581 , 1095 , 594 , and 532 cm^{-1} . The peak at 1581 cm^{-1} may correspond to the amide bending vibration of proteins N-H bond or may be due to the stretching vibration of aromatic C=C bonds [12]. The next observed peaks at 1095 cm^{-1} could be caused by aliphatic ether C-O

stretching [12]. The two strong peaks of stretching vibration at 594 and 532 cm^{-1} correspond to Fe-O bond formation in Fe_2O_3 NRs [13-14].

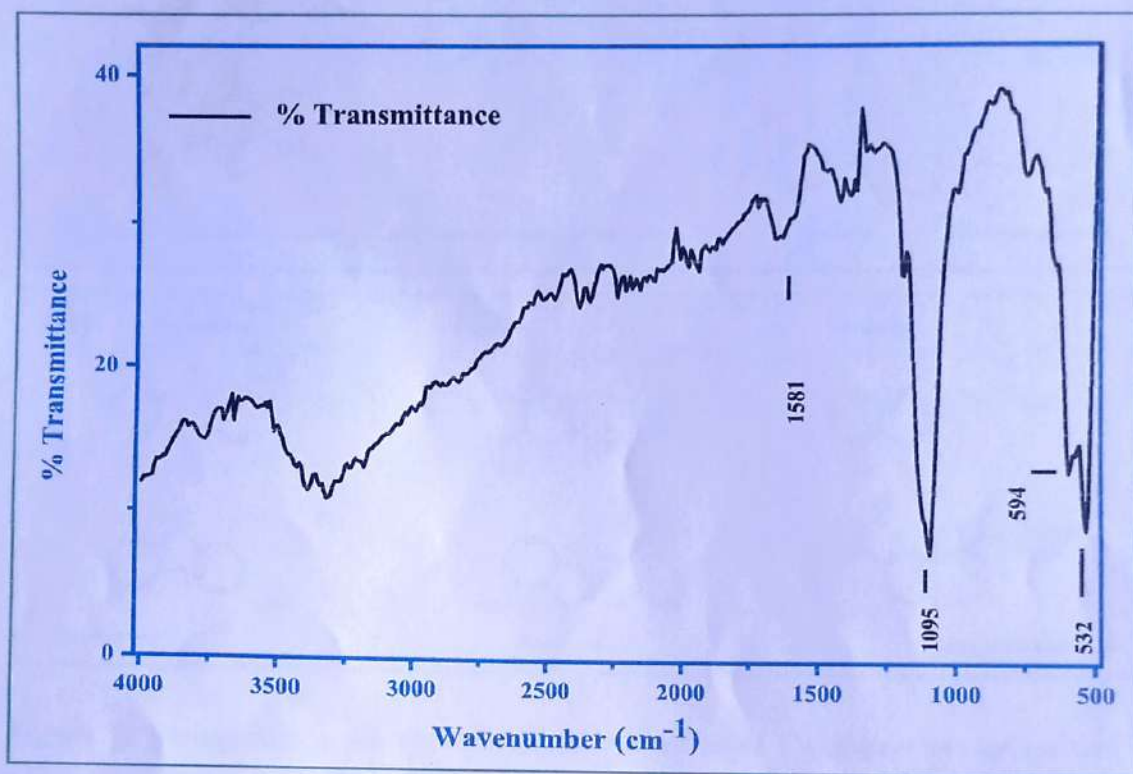


Figure 4: FTIR spectrum of biosynthesized Fe_2O_3 NRs

Figure 5 illustrates the main active phytochemicals found in *Eucalyptus citriodora* (**Fig. 5a**), and *Murraya koenigii* (**Fig. 5b**) leaves to explain how the metal precursor salt $\text{Fe}(\text{NO}_3)_2 \cdot 9 \text{H}_2\text{O}$ can change into Fe_2O_3 nanorods. The plausible reaction mechanism demonstrates how different active phytochemicals act as stabilizing and reducing agents. Diverse active phytochemicals are found in *Eucalyptus citriodora* and *Murraya koenigii*, including saponins, carbohydrates, sterols, glycosides, alkaloids, flavonoids, terpenoids, and polyphenols [15-16]. For a possible reaction mechanism, a flavonoid has been chosen as a sample molecule to suggest the mechanism. Because of the electrostatic attraction between hydroxyl groups of flavonoid and cation of metal precursor, aromatic hydroxyl groups bind to ferric ions (Fe^{3+}), and ferric ions and flavonoids form a stable complex. After the treatment of calcination, the complex decomposes and forms Fe_2O_3 nanorods. As a result, the single-phase formation of Fe_2O_3 is not selective. Therefore, two phases were observed in the XRD analysis corresponding to $\alpha\text{-Fe}_2\text{O}_3$ and $\gamma\text{-Fe}_2\text{O}_3$ (**Figure 6**).

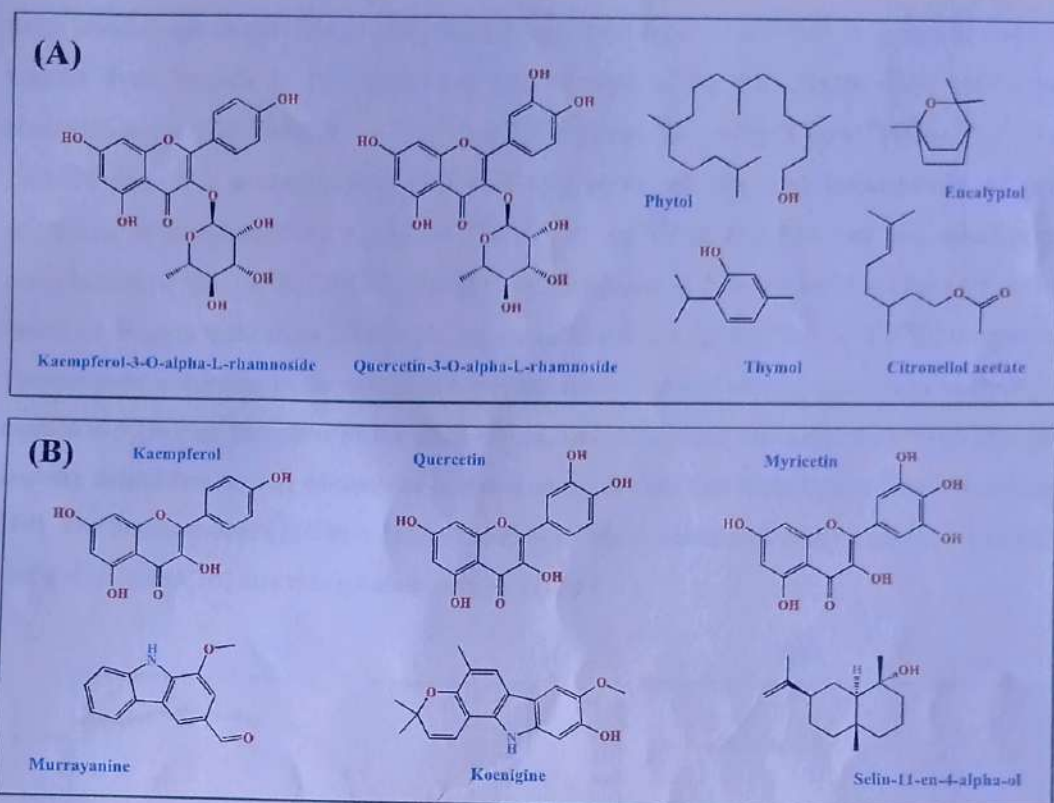


Figure 5: Biologically active phytochemicals present in a) *Eucalyptus citriodora* and b) *Murraya koenigii*

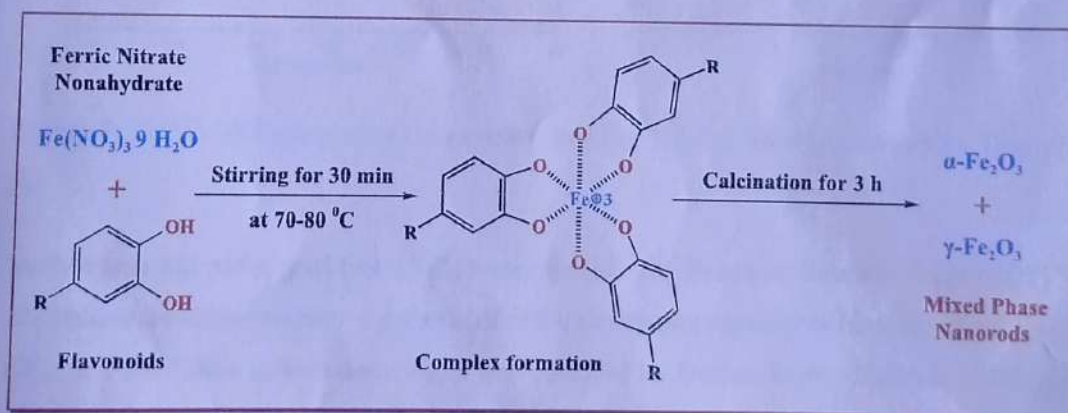


Figure 6: A plausible reaction mechanism for the formation of Fe_2O_3 NRs using metal salt and leaf extracts

The optical absorbance of the fabricated mixed-phase Fe_2O_3 NRs ($\alpha\text{-Fe}_2\text{O}_3$ -Hematite and $\gamma\text{-Fe}_2\text{O}_3$ -Maghemite) was investigated in the range of 200 to 800 nm [17]. The corresponding spectrum is shown in Figure 7a. The absorption spectra of a Fe_2O_3 NRs show the presence of

three distinct adsorption zones [18], namely, the first region (200-400 nm) due to charge-transfer from ligands to Fe^{3+} metal ion and because of the Fe^{3+} ligand field transitions contributions, in part from ${}^6\text{A}_1 \rightarrow {}^4\text{T}_1({}^4\text{P})$ at 290-310 nm, ${}^6\text{A}_1 \rightarrow {}^4\text{E}({}^4\text{D})$ and ${}^6\text{A}_1 \rightarrow {}^4\text{T}_2({}^4\text{D})$ at 360-380 nm. The second region (400-600 nm) represents the end consequence of pair excitation of processes ${}^6\text{A}_1 + {}^6\text{A}_1 \rightarrow {}^4\text{T}_1({}^4\text{G}) + {}^4\text{T}_1({}^4\text{G})$ at 485-550 nm and overlapped contribution of ${}^6\text{A}_1 \rightarrow {}^4\text{E}$, ${}^4\text{A}_1({}^4\text{G})$ ligand field transitions at 430 nm and the charge-transfer band tail. Region third (600-750 nm) is attributed to 640 nm for the ${}^6\text{A}_1 \rightarrow {}^4\text{T}_2({}^4\text{G})$ transition. Furthermore, according to the selection rules, the area's first and second absorption intensity is significantly higher than that of the third region, indicating that the absorption from charge-transfer transitions or pair excitations is much stronger than that from ligand field transitions [19]. The bandgap energy of biosynthesized Fe_2O_3 NRs is calculated using Tauc's plot (direct method) (Figure 7b) and was estimated to be 2.02 eV.

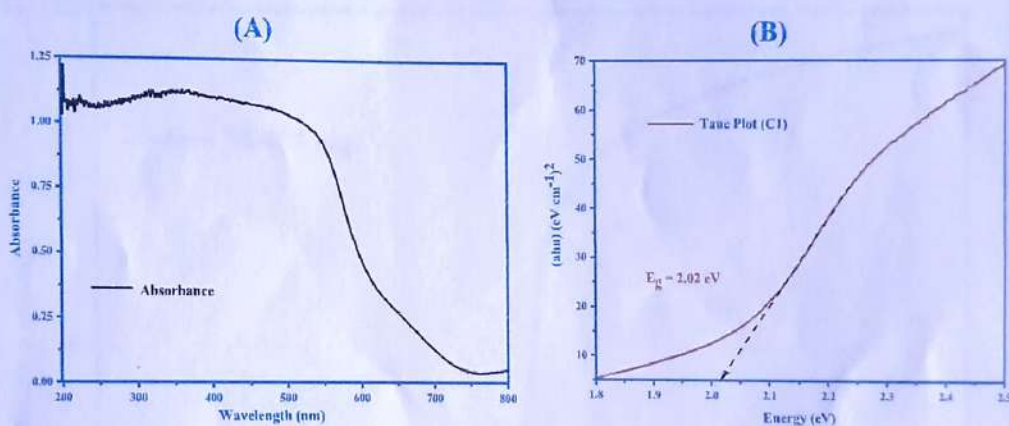


Figure 7: a) UV-DRS spectrum of bio-synthesized Fe_2O_3 NRs; Band-gap energy by Tauc plot (b)

Surface area and porosity of Fe_2O_3 NRs were calculated by Brunauer-Emmett-Teller (BET) N_2 adsorption/desorption studies to get an idea of the absorbance capacity of biosynthesized Fe_2O_3 NRs, and Pore Size distribution (PSD) was obtained by Barrett-Joyner-Halenda (BJH) plot (Figure 8). The surface area of the as-formulated sample was observed to be $16.13 \text{ m}^2 \text{ g}^{-1}$.

The magnetic behavior of biosynthesized Fe_2O_3 NRs was investigated by Vibrating Sample Magnetometry (VSM). Figure 9 shows the hysteresis loop for synthesized Fe_2O_3 NRs. The value of M_s , H_c , and M_r (Table 2) were estimated based on the hysteresis loop by applying the applied field in the range of -15 kOe to 15 kOe to study the magnetic characteristics of NRs.

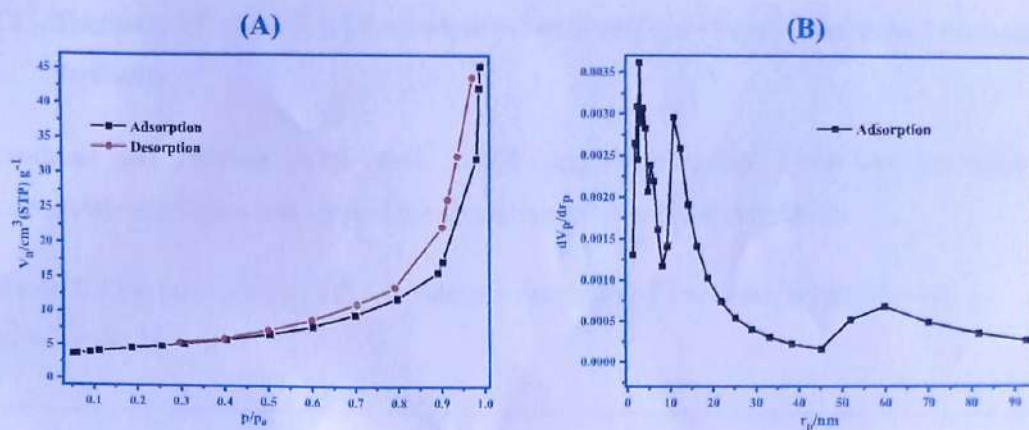


Figure 8: a) Nitrogen adsorption-desorption isotherms at -196 °C (BET plot); b) Pore size distribution plot of Fe_2O_3 NRs (BJH plot)

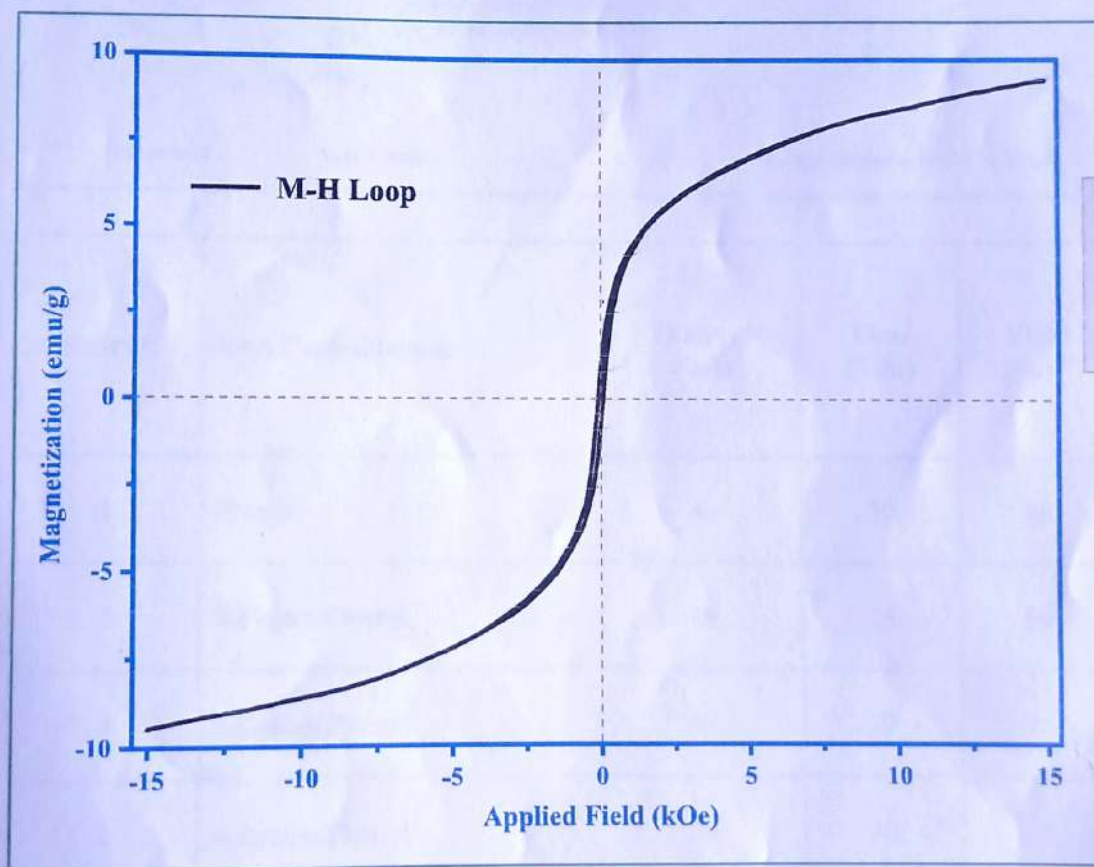


Figure 9: VSM plot of biosynthesized Fe_2O_3 NRs

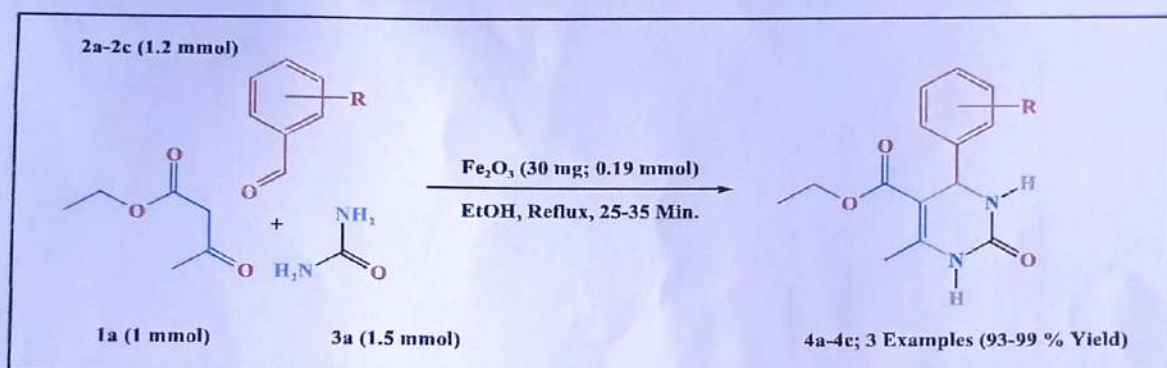
Saturation magnetization (Ms)	Coercivity (Hc)	Remnant field (Mr)
09.39 emu/g	78.98 Oe	0.84 emu/g

Table 2: Summary for Magnetic properties of biosynthesized Fe_2O_3 NRs

3.2 Synthesis of ethyl 1,2,3,4-tetrahydro-6-methyl-2-oxo-4-arylpyrimidine-5-carboxylate derivative

Synthesis and purification of ethyl 1,2,3,4-tetrahydro-6-methyl-2-oxo-4-arylpyrimidine-5-carboxylate derivative was carried out according to section 2.4 procedure.

Table 3: Synthesis of ethyl 1,2,3,4-tetrahydro-6-methyl-2-oxo-4-arylpyrimidine-5-carboxylate derivative



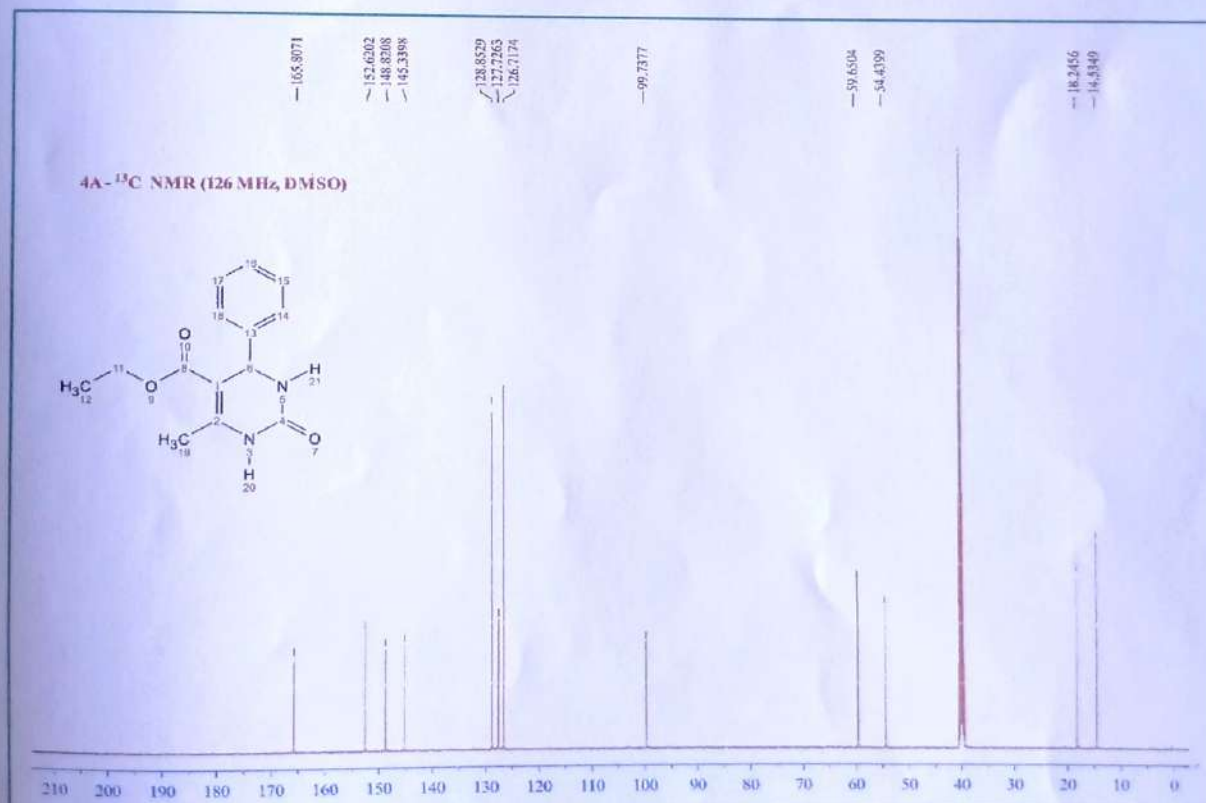
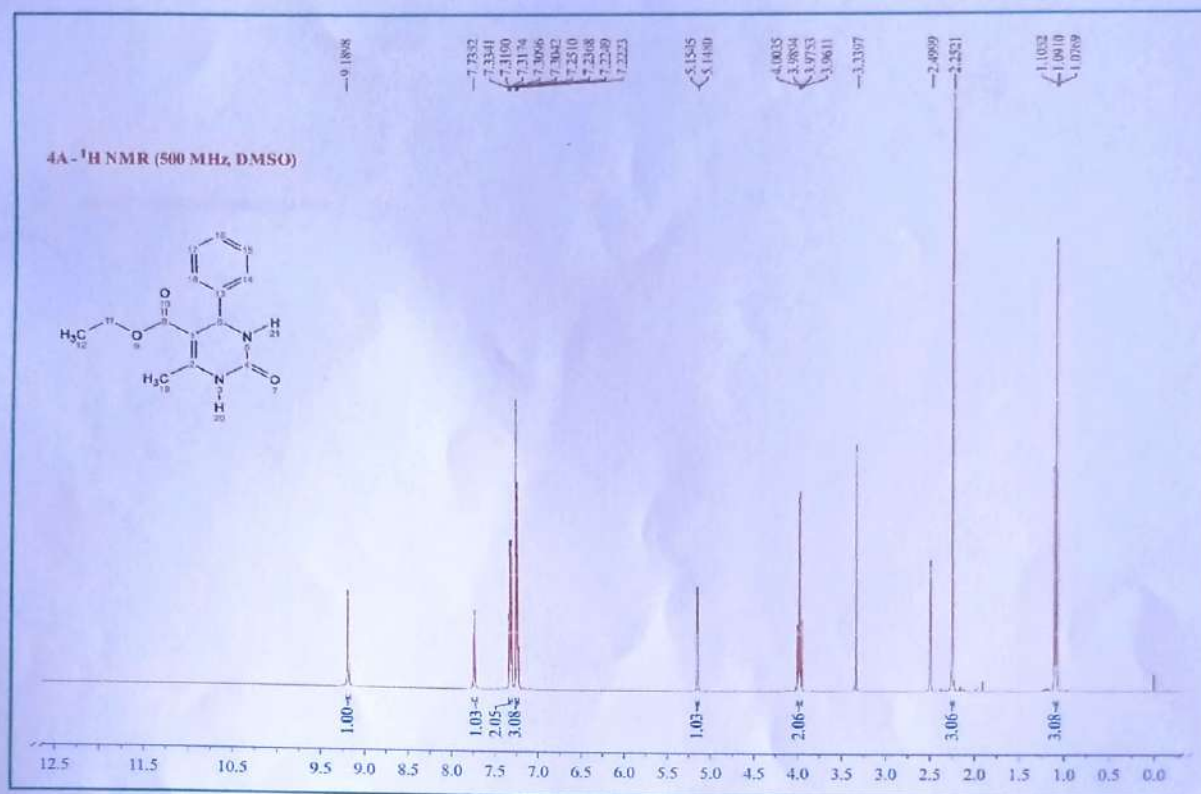
Entry ^a	Aryl Carbaldehyde	Product Code	Time (Min)	Yield (%) ^b
1	Phenyl	4a	30	95
2	4-Fluoro Phenyl	4b	25	94
3	4-Chloro Phenyl	4c	27	96
4	4-Bromo Phenyl	4d	30	95

^a Reaction Condition: Ethyl acetoacetate (1 mmol), Aromatic aldehyde (1.2 mmol), Urea (1.5 mmol), Ethanol (3 ml), Catalyst- Fe_2O_3 NRs (30 mg; 0.19 mmol; 4.83 mol %) under reflux condition.

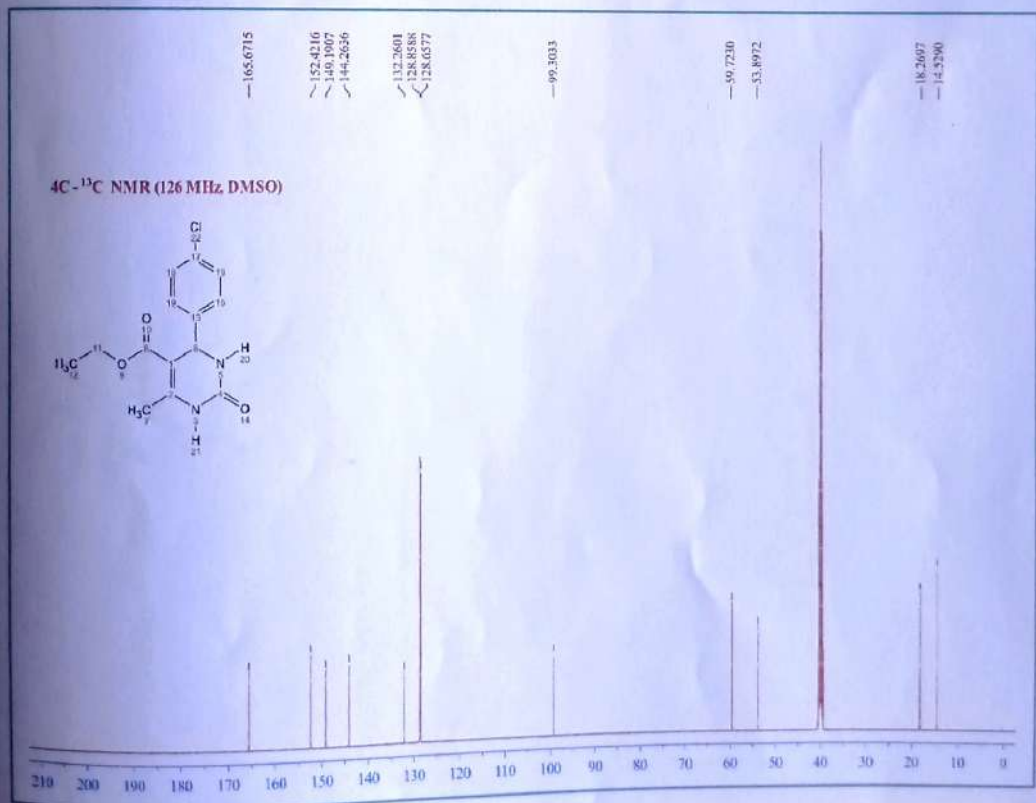
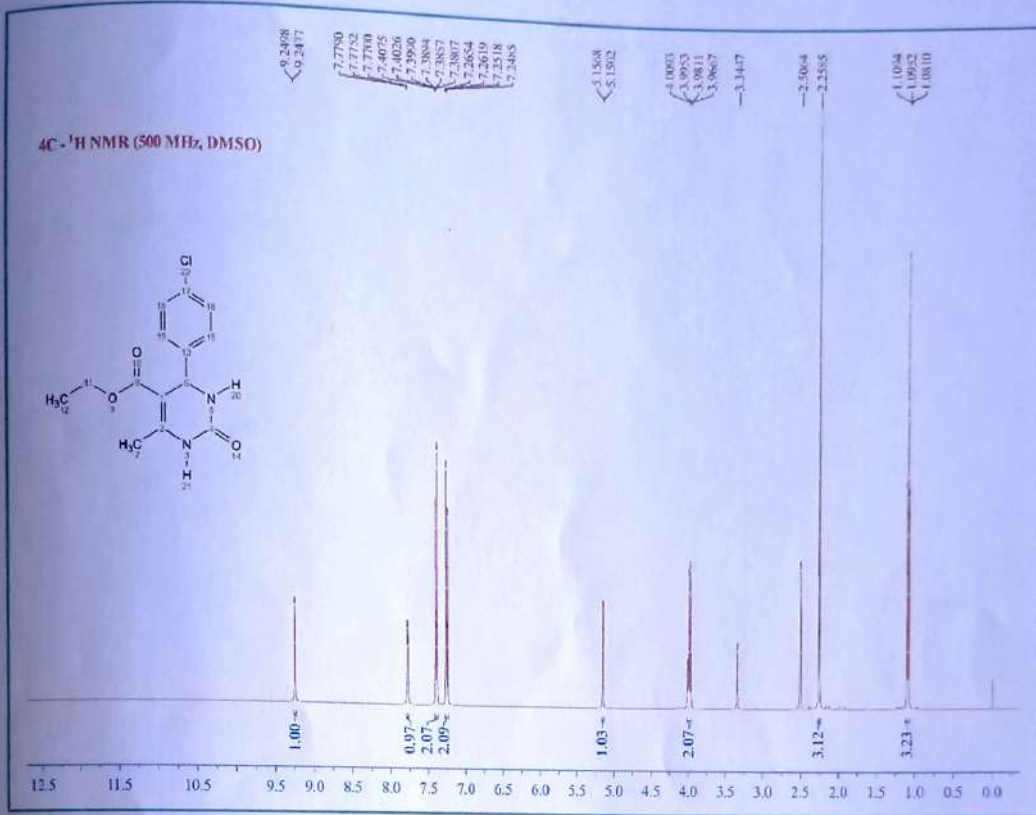
^b Isolable yield

Spectra data of synthesized compounds are as follows:

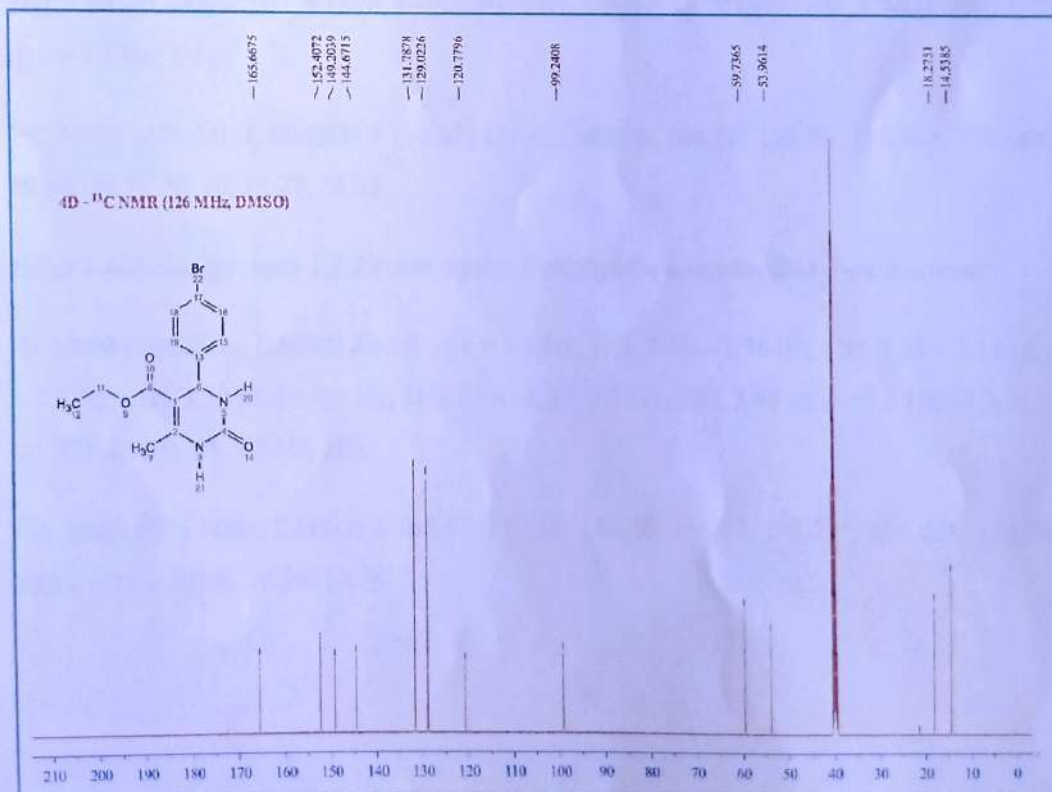
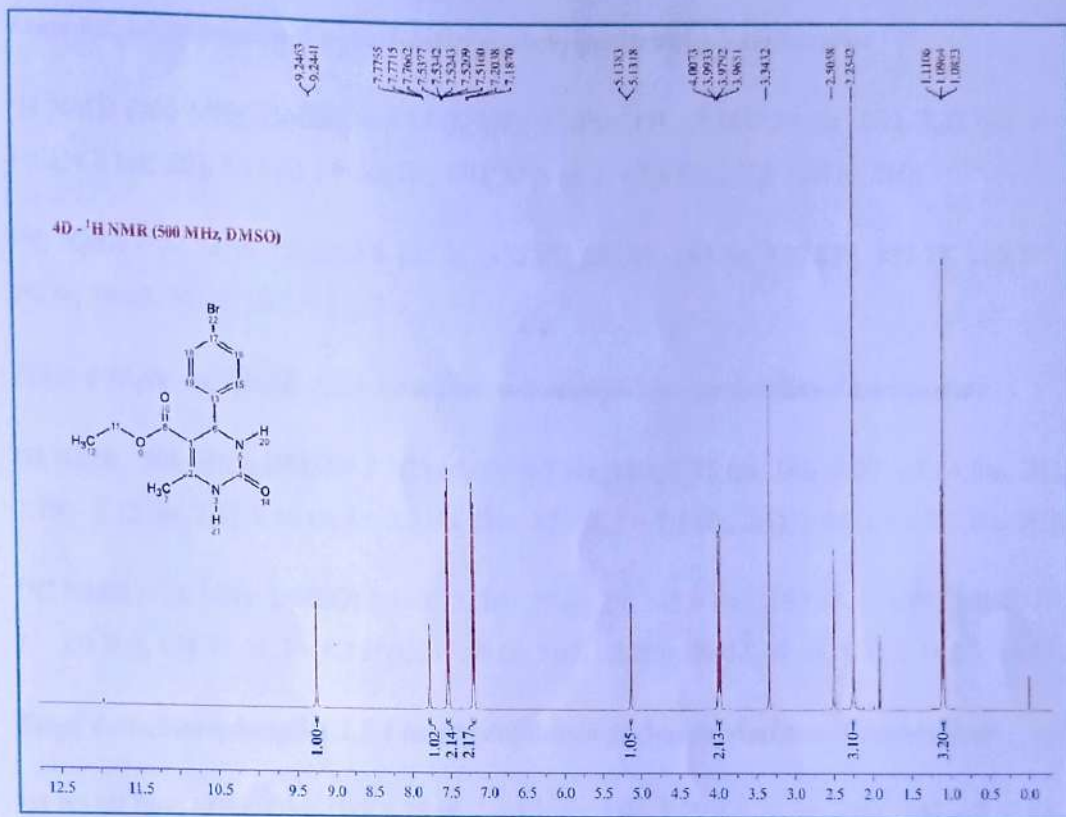
Ethyl 1,2,3,4-tetrahydro-6-methyl-2-oxo-4-phenylpyrimidine-5-carboxylate



Ethyl 4-(4-chlorophenyl)-1,2,3,4-tetrahydro-6-methyl-2-oxopyrimidine-5-carboxylate



Ethyl 4-(4-bromophenyl)-1,2,3,4-tetrahydro-6-methyl-2-oxopyrimidine-5-carboxylate



Spectral Data Analysis:

Ethyl 1,2,3,4-tetrahydro-6-methyl-2-oxo-4-phenylpyrimidine-5-carboxylate

¹H NMR (500 MHz, DMSO) δ 9.19 (s, 1H), 7.74 (s, 1H), 7.34-7.30 (m, 2H), 7.23 (dd, J = 10.2, 4.2 Hz, 3H), 5.15 (d, J = 3.3 Hz, 1H), 3.98 (q, J = 7.1 Hz, 2H), 2.25 (s, 3H);

¹³C NMR (126 MHz, DMSO) δ 165.81, 152.62, 148.82, 145.34, 128.85*, 127.73, 126.72*, 99.74, 59.65, 54.44, 18.25, 14.53.

Ethyl 4-(4-fluorophenyl)-1,2,3,4-tetrahydro-6-methyl-2-oxopyrimidine-5-carboxylate

¹H NMR (500 MHz, DMSO) δ 9.23 (d, J = 0.7 Hz, 1H), 7.75 (m, 1H), 7.29 – 7.24 (m, 2H), 7.18 – 7.12 (m, 2H), 5.16 (d, J = 3.2 Hz, 1H), 3.98 (t, J = 7.1 Hz, 2H), 1.09 (t, J = 7.1 Hz, 3H);

¹³C NMR (126 MHz, DMSO) δ 165.72, 161.79 (d, J = 242.9 Hz), 152.45, 148.99, 141.60 (d, J = 3.0 Hz), 128.71 (d, J = 8.2 Hz), 115.58 (d, J = 21.3 Hz), 99.60, 59.68, 53.82, 18.25, 14.52.

Ethyl 4-(4-chlorophenyl)-1,2,3,4-tetrahydro-6-methyl-2-oxopyrimidine-5-carboxylate

¹H NMR (500 MHz, DMSO) δ 9.25 (d, J = 1.1 Hz, 1H), 7.79 – 7.76 (m, 1H), 7.41 – 7.38 (m, 2H), 7.28 – 7.24 (m, 2H), 5.15 (d, J = 3.3 Hz, 1H), 3.99 (q, J = 7.1 Hz, 2H), 2.26 (s, 3H), 1.10 (t, J = 7.1 Hz, 3H);

¹³C NMR (126 MHz, DMSO) δ 165.67, 152.42, 149.19, 144.26, 132.26, 128.86*, 128.66*, 99.30, 59.72, 53.90, 18.27, 14.53.

Ethyl 4-(4-bromophenyl)-1,2,3,4-tetrahydro-6-methyl-2-oxopyrimidine-5-carboxylate

¹H NMR (500 MHz, DMSO) δ 9.25 (d, J = 1.1 Hz, 1H), 7.78 – 7.76 (m, 1H), 7.55 – 7.51 (d, J = 8.4 Hz, 2H), 7.20 (d, J = 8.4 Hz, 2H), 5.14 (d, J = 3.3 Hz, 1H), 3.99 (q, J = 7.1 Hz, 2H), 2.25 (s, 3H), 1.10 (t, J = 7.1 Hz, 3H);

¹³C NMR (126 MHz, DMSO) δ 165.67, 152.41, 149.20, 144.67, 131.79*, 129.02*, 120.78, 99.24, 59.74, 53.96, 18.28, 14.54.

3.3 Probable mechanistic pathway of the reaction

Various theoretical and experimental discussions have been reported for the mechanistic pathway of the Biginelli reaction. The three mechanistic pathways have been proposed based on the intermediate involved in the reaction (Figure 10).

The first mechanistic path is the iminium route (Figure 10a) [20], which involves condensation of aldehyde and urea to get iminium intermediate, on which nucleophilic addition of ethyl 3-hydroxybut-2-enoate (enol generated in-situ from Ethyl acetoacetate) leads to the formation of THPMs. The second mechanistic path is via the enamine route (Figure 10b) [21]. It involves condensation of β -keto ester and urea leads to protonated enamine intermediate, which subsequently undergoes nucleophilic addition on aldehyde to get THPMs. The third mechanistic path involves a Knoevenagel-type reaction (Figure 10c) [22]. Here firstly, the condensation of an aldehyde with ethyl 3-hydroxybut-2-enoate (enol generated in-situ from Ethyl acetoacetate) takes place, which on reaction with urea result in the formation of THPMs. In the last decade, De Souza et al. [23], Neto et al. [24], and Puripat et al. [25] did a comparative study on the mechanistic path of the Biginelli reaction. They found that the Iminium intermediate route is favored over the Enamine and Knoevenagel route. According to Puripat et al. [25], based on AFIR and DFT calculation, the order of reactive intermediate formation is Imine > Enamine > Knoevenagel route.

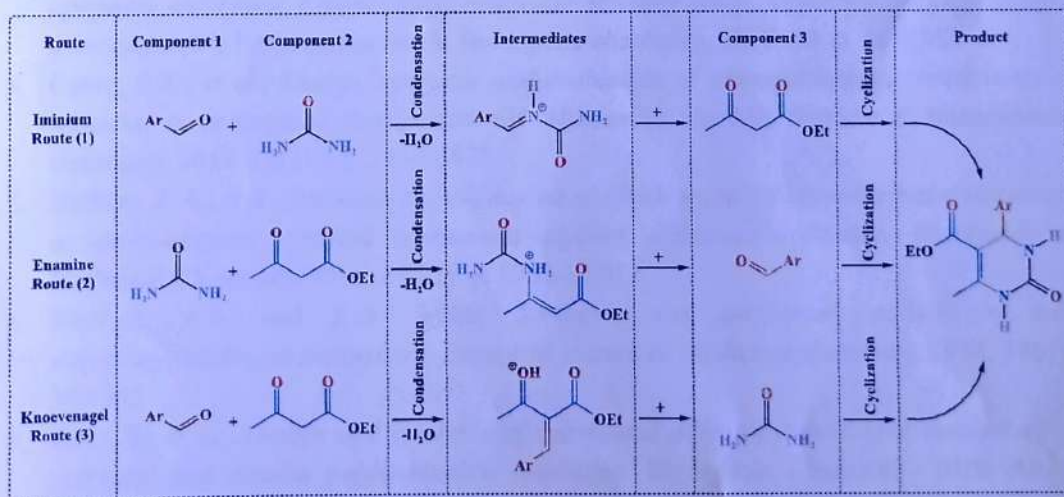


Figure 10. Possible reaction mechanism for the Fe₂O₃ NRs catalyzed THPMs synthesis

4. Conclusion

In this study, for the first time, mixed-phase Fe₂O₃ NRs were biologically synthesized using a mixture of *Eucalyptus citriodora* and *Murraya koenigii* leaf extracts and its application as a heterogeneous magnetic nanocatalyst in the multicomponent Biginelli reaction was reported. The catalyst was synthesized through an utterly green approach and then characterized by XRD, UVDRS, FTIR, FESEM, EDX, and VSM analysis. Then, the practical synthesis of ethyl 1,2,3,4-tetrahydro-6-methyl-2-oxo-4-arylpyrimidine-5-carboxylate was prepared with an ethyl acetoacetate, aromatic aldehydes, urea with a catalytic amount of the magnetically recoverable Fe₂O₃ NRs in ethanol as a green solvent. The notable merits of this protocol are easy workup procedure, reusability of catalyst, being clean and safe and having excellent yields of the final products. This eco-friendly approach for synthesizing Fe₂O₃ NRs can open new horizons for exploring their possible role in organic transformation.

References

1. Kim, J., et al., *A novel 3, 4-dihydropyrimidin-2 (1H)-one: HIV-1 replication inhibitors with improved metabolic stability*. Bioorganic & medicinal chemistry letters, 2012. **22**(7): p. 2522-2526.
2. de Fátima, Â., et al., *A mini-review on Biginelli adducts with notable pharmacological properties*. Journal of advanced research, 2015. **6**(3): p. 363-373.
3. Janković, N., et al., *Discovery of the Biginelli hybrids as novel caspase-9 activators in apoptotic machines: Lipophilicity, molecular docking study, influence on angiogenesis gene and miR-21 expression levels*. Bioorganic chemistry, 2019. **86**: p. 569-582.
4. Canto, R.F., et al., *Design, synthesis and evaluation of seleno-dihydropyrimidinones as potential multi-targeted therapeutics for Alzheimer's disease*. Organic & biomolecular chemistry, 2014. **12**(21): p. 3470-3477.
5. Barbosa, F.A., et al., *Synthesis and evaluation of dihydropyrimidinone-derived selenoesters as multi-targeted directed compounds against Alzheimer's disease*. Bioorganic & Medicinal Chemistry, 2016. **24**(22): p. 5762-5770.
6. Mostafa, A.S. and K.B. Selim, *Synthesis and anticancer activity of new dihydropyrimidinone derivatives*. European journal of medicinal chemistry, 2018. **156**: p. 304-315.
7. Sana, S., et al., *Design and synthesis of substituted dihydropyrimidinone derivatives as cytotoxic and tubulin polymerization inhibitors*. Bioorganic Chemistry, 2019. **93**: p. 103317.
8. Tungittiplakorn, W., C. Cohen, and L.W. Lion, *Engineered polymeric nanoparticles for bioremediation of hydrophobic contaminants*. Environmental Science & Technology, 2005. **39**(5): p. 1354-1358.
9. Pauling, L. and S.B. Hendricks, *The crystal structures of hematite and corundum*. Journal of the American Chemical Society, 1925. **47**(3): p. 781-790.

10. Hmamouchi, S., A. El Yacoubi, and B.C. El Idrissi, *Using egg ovalbumin to synthesize pure α -Fe₂O₃ and cobalt doped α -Fe₂O₃: structural, morphological, optical and photocatalytic properties*. Heliyon, 2022. **8**(2): p. e08953.
11. Pecharromán, C., T. Gonzalez-Carreno, and J.E. Iglesias, *The infrared dielectric properties of maghemite, γ -Fe₂O₃, from reflectance measurement on pressed powders*. Physics and Chemistry of Minerals, 1995. **22**(1): p. 21-29.
12. Fouda, A., et al., *An eco-friendly approach to textile and tannery wastewater treatment using maghemite nanoparticles (γ -Fe₂O₃-NPs) fabricated by Penicillium expansum strain (Kw)*. Journal of Environmental Chemical Engineering, 2021. **9**(1): p. 104693.
13. Ali, H.R., H.N. Nassar, and N.S. El-Gendy, *Green synthesis of α -Fe₂O₃ using Citrus reticulum peels extract and water decontamination from different organic pollutants*. Energy Sources, Part A: Recovery, Utilization, and Environmental Effects, 2017. **39**(13): p. 1425-1434.
14. Miri, A., M. Khatami, and M. Sarani, *Biosynthesis, magnetic and cytotoxic studies of hematite nanoparticles*. Journal of Inorganic and Organometallic Polymers and Materials, 2020. **30**(3): p. 767-774.
15. Zhou, Z.-L., et al., *Flavonoid glycosides and potential antiviral activity of isolated compounds from the leaves of Eucalyptus citriodora*. Journal of the Korean Society for Applied Biological Chemistry, 2014. **57**: p. 813-817.
16. Ibrahim, J., et al., *Comparative pharmacognostic and chemical analyses of Eucalyptus camaldulensis Dehnh and Eucalyptus citriodora (Hook)*. Journal of Chemical Society of Nigeria, 2018. **43**(3).
17. Nejres, A.M., et al., *Potential effect of ammonium chloride on the optical physical properties of polyvinyl alcohol*. Systematic Reviews in Pharmacy, 2020. **11**(6): p. 726-732.
18. He, Y., et al., *Size and structure effect on optical transitions of iron oxide nanocrystals*. Physical review B, 2005. **71**(12): p. 125411.
19. Apriandanu, D.O.B., et al., *Effect of two-step annealing on photoelectrochemical properties of hydrothermally prepared Ti-doped Fe₂O₃ films*. Catalysis Today, 2022.
20. Kappe, C.O., *A reexamination of the mechanism of the Biginelli dihydropyrimidine synthesis. Support for an N-Acyliminium ion intermediate*. The Journal of organic chemistry, 1997. **62**(21): p. 7201-7204.
21. Folkers, K. and T.B. Johnson, *Researches on pyrimidines. CXXXVI. the mechanism of formation of tetrahydropyrimidines by the biginelli reaction*. Journal of the American Chemical Society, 1933. **55**(9): p. 3784-3791.
22. Sweet, F. and J.D. Fissekis, *Synthesis of 3, 4-dihydro-2 (1H)-pyrimidinones and the mechanism of the Biginelli reaction*. Journal of the American Chemical Society, 1973. **95**(26): p. 8741-8749.
23. De Souza, R.O., et al., *The three-component Biginelli reaction: a combined experimental and theoretical mechanistic investigation*. Chemistry—A European Journal, 2009. **15**(38): p. 9799-9804.
24. dos Santos, R.L.T.A., *MR de Oliveira HCB Gomes AF Gozzo FC de Oliveira AL Neto BAD J. Org. Chem*, 2012. **77**: p. 10184-10193.
25. Puripat, M., et al., *The Biginelli reaction is a urea-catalyzed organocatalytic multicomponent reaction*. The Journal of Organic Chemistry, 2015. **80**(14): p. 6959-6967.